Causality-informed Bayesian Inference for Rapid Seismic Ground Failure and Building Damage Estimation

S. Xu[1], D. J. Wald[2], J. T. Dimasaka[3], H. Y. Noh[4]

ABSTRACT

Rapid and accurate estimates of seismic ground failure and building damage are beneficial to efficient emergency response and post-earthquake recovery. Traditional approaches, such as physical and geospatial models, have limited accuracy and resolution due to large uncertainties and the limited availability of informing geospatial layers. The introduction of remote sensing techniques has shown the potential to provide supplementary information for rapid hazard estimation through analyzing earthquake-induced correlation changes between pre- and post-event satellite images. Nevertheless, the changes in satellite images are the result of overlapping ground failure, building damage, and environmental noise, making it challenging to categorize and estimate different seismic hazards and impacts directly from satellite images. Here we design a novel causal graph-based Bayesian network that continuously updates seismic ground failure and building damage estimates from satellite images by modeling the physical interdependencies between geospatial features, ground shaking, ground failure, building footprints, and building damage, as well as satellite images. The key approach is based on the idea that there exist physical interdependencies among multiple natural hazardous geological processes, and thus incorporation of the physical interdependencies allows an effective fusion of physical insights from existing USGS models and rich but noisy information from remote sensing observations, e.g., Damage Proxy Maps (DPMs), and further reduces bias and uncertainties in estimations. The framework introduced provides a scalable and flexible way to deal with highly complex multi-hazard scenarios. Our experiments show that integrating satellite images through Bayesian network improves estimation accuracy.

Introduction

Earthquake-induced ground failures and building damage cause significant economic losses and fatalities. For example, the 2008 Wenchuan earthquake in China triggered about 200,000 landslides, leading to around 26,500 deaths [1] in addition to nearly 60,000 shaking-induced fatalities. The series of earthquakes in Christchurch, New Zealand, in 2011, induced liquefaction of over one-third of the city, affecting more than 6,000 buildings and resulting in enormous economic costs [2]. These induced hazards have been shown to cause disruption to lifelines and structural damage to buildings [3]. Therefore, rapidly and accurately localizing and estimating ground failure and damage occurrences are beneficial to effective and efficient response and recovery.

[1]Assistant Professor, Dept. of Civil Engineering, Stony Brook University, Stony Brook, NY 11794
[2]Geophysicist, U.S. Geological Survey, National Earthq. Information Center, Golden, CO 80401 (email: wald@usgs.gov)
[3]Graduate Student Researcher, Dept. of Civil Engineering, Stanford University, Stanford, CA 80401
[4]Associate Professor, Dept. of Civil and Environmental Engineering, Stanford University, Stanford, CA 94305

Most existing approaches for earthquake-induced ground failure and building damage estimation suffer from low performance due to outdated data, region-specific trends, and environmental noises. Current practices by the USGS utilize statistical models calibrated against patterns of past ground failures using historical inventories given geospatial susceptibility proxies (including slope, lithology.) and ground motion to estimate single-type ground failure modes separately [4]. The resolution and accuracy of these statistical models are often constrained by the limited availability of geospatial features as well as modeling uncertainties. For example, it is difficult to acquire comprehensive high-resolution lithology, land cover type, and other predictor variables for landslide model susceptibility, or soil strength and water depth needed for liquefaction modeling.

Recently, remote sensing techniques have been developed to capture satellite images before and after an earthquake and difference them. Damage Proxy Maps (DPMs) are further extracted based on coherences between satellite images to indicate earthquake-induced ground surface changes [5]. Nevertheless, it is difficult to categorize different types of changes through these imagery data, such as ground failure, building damage, and noise from vegetation growth and anthropogenic modifications, especially when these changes co-occur [6]. Some prior studies incorporated geospatial features and remote sensing observations for estimating single-type ground failure using linear combinations or black-box supervised classifiers [7, 8]. However, these approaches lack consideration of complex and event-varying physical interdependencies among multiple co-occurring ground failure types and building damage, which limit their applicability for common multi-hazard, mixed-signal scenarios.
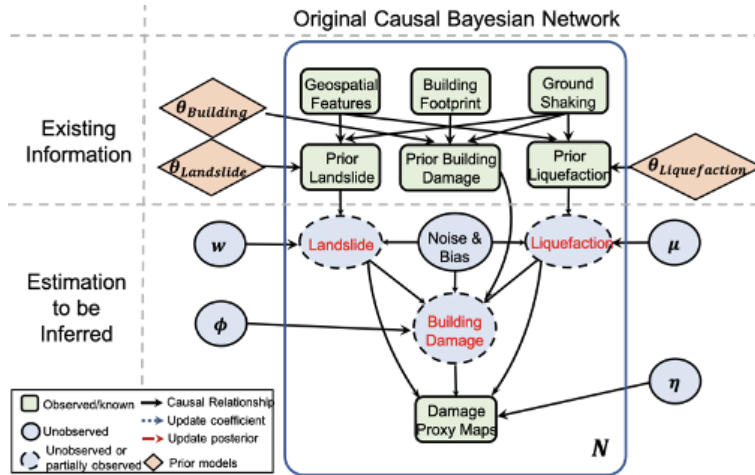

Figure 1. Overview of the posterior and model updating based on causal Bayesian network.

In this work, we introduce a causal Bayesian network framework integrating geospatial models with DPMs through a physics-informed causal graph for fast and effective joint estimation of regional ground failure and building damage. The Bayesian network uses a probabilistic causal graph as the foundation for encoding a set of conditional dependency relationships among multiple variables, e.g., physical causal relationships among multiple geospatial features, ground failures, building footprints, building damage, and DPMs, as shown in Fig. 1. To infer posterior distributions from the complex probabilistic graph, we build our algorithm on variational inference, which is a powerful statistical machine learning technique for inferring complex probabilistic models with many unobserved variables [9]. A new stochastic variational inference algorithm is further designed to jointly approximate the posterior distributions of unobserved ground failures and building damage, as well as their statistical correlations, by maximizing the lower bound of the likelihood of observed DPMs. The algorithm is also flexible enough to incorporate new ground truth information of ground failures and building damage.

Methodology

We design a causal graph to best depict and approximate the causally linked earthquake-induced hazards. The original causal graph is built based on causal relationships among ground failure, building damage, geospatial features, ground shaking, Damage Proxy Maps (DPMs), and environmental noises. As shown in Fig.1, nodes refer to different types of hazards and observations, and edges represent causal relationships between them. Earthquake ground shaking, triggers landslides and liquefaction, and ground shaking, landslides, and liquefaction further result in building damage. Environmental noises, such as subtle environmental factors that are not predicted by geospatial features, also contribute to DPM signals. Finally, ground failure, building damage, and environmental noises which all lead to ground surface changes captured by DPMs, must be distinguished from each other.

Specifically, given one location (i.e., one pixel in DPMs), we first denote x_1 for landslide (LS), x_2 for liquefaction (LF), and x_3 for building damage (BD). Landslide and liquefaction are initially completely unobserved variables and thus are assumed to have categorical distributions. The unobserved ground failure nodes have categorical variables where $x_i \in \{0, 1, \cdots, M\}$, where $i \in \{1, 2, 3\}$. For example, if M = 1, when the LS/LF happen, $x_i = 1$, otherwise $x_i = 0$. Or if M = 4 for building damage, x_3 is a categorical distribution representing five different damage states: no damage, slight damage, moderate damage, severe damage, and collapse. We use y to refer to pixel-wise *DPM* observation, which is a continuous variable bounded by [0,1]. We denote g_k as observed geospatial features and denote ϵ_i, ϵ_y as unobserved Gaussian noise in LS, LF, and BD, as well as in DPMs, respectively. We define $w_0, \mu_0, \phi_0, \theta_{0k}, and \eta_0$ to model the bias contained in LS, LF, BD, geospatial features, and DPMs. To simplify the notation, we define u_{ϵ_i} and u_{ki} (k is any parent node of i) to quantify the correlations between the noise term and node i as well as between the parent node k and node i. When $i = 1, 2, 3, y, u_{ki} = w_k, \mu_k, \phi_k, \eta_k$, respectively. All above nodes will be formulated as deterministic variables.
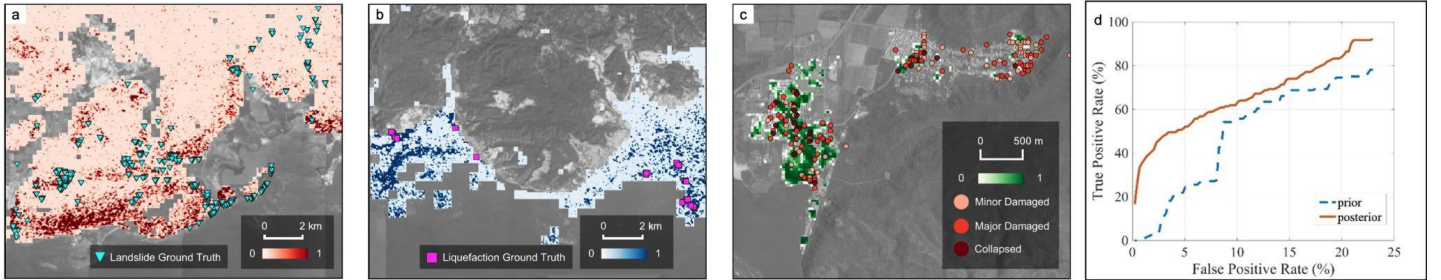

Figure 2. Evaluation on the January 2020 Puerto Rico earthquake: (a) our posterior landslide estimations, (b) our posterior liquefaction estimations, (c) our posterior building damage estimations, and (d) ROC curves of prior and posterior liquefaction model.

All nodes are linked by an arbitrary directed acyclic graph in Fig. 1. We further give quantitative definitions of these links, i.e., statistical relationships, between different random variables. For example, even if neither landsliding nor liquefaction is present, building damage is still possible due to the shaking. Using $P(i)$ to represent the parents of node i (excluding the leaf nodes x_0 and ϵ_i), the distribution of x_i is modeled as:

$$log \frac{p(x_{P(i)}=m,\epsilon_i)}{1-p(x_{P(i)}=m,\epsilon_i)} = u_{\epsilon_i}\epsilon_i + u_{0i}x_0 + \sum_{k \in P(i)} u_{ki}x_k. \tag{1}$$

For LS/LF/BD, the above logit relationship models the dependencies between the nodes and their parent nodes following the assumption of the logistic regression model used by the USGS [10, 11]. If all parents are active ($x_k = 1; \forall k \in P(i)$), they activate the child node i regardless of the states of other parents. If $x_k = 0$, parent k has no influence on the state of x_i. $u_{\epsilon_i}\epsilon_i$ measures noise in the dependencies. $u_{0i}x_0$ helps estimate and cancel the bias introduced by prior models. Given the M classes (i.e., multinoulli distribution), the joint probability is further modeled as:

$$p\left(x_{P(i)}, \epsilon_i\right) = \prod_{m=1}^{M} \left[p\left(x_{P(i)} = m, \epsilon_i\right)\right]^{x_i}, \tag{2}$$

Given y, we use $P(y)$ to define the parents of y. Based on the empirical probability density function of DPMs, we found y subjects to a truncated lognormal distribution bounded by [0, 1] with:

$$log\,(y + \delta) \ = u_{\epsilon_y} \epsilon_y + u_{0y} + \sum_{i \in P(y)} u_{iy} x_i, \tag{3}$$

where ϵ_y is a normal distribution representing the random noise in the DPM, $u_{0y} \le 0$ estimates regional bias, $\delta \rightarrow 0^+$, and $y|\,P(y)$ has a truncated log-normal distribution.

For each location $l \in L$, where L refers to the entire seismic zone, we define a variational distribution $q\left(X^l\right)$ which further factorizes over hidden (unobserved) nodes. At each geo-location, q_i^l is defined to approximate the posterior probability that node i at location l is active, for example, q_{LS}^l refers to the probability of landslide occurrence at the location l. For any $q\left(X^l\right)$, the joint log-likelihood of the observed DPMs (y^l) can be lower bounded by factorizing the Bayesian network with a set of posterior distributions of unobserved random variables (e.g., landslide, liquefaction, building damage, and noise) as follows:

$$log\,p\left(y^l\right) \ \ge E_{q\left(X^l\right)}\left[log\,p(X^l, y^l) - log\,q\left(X^l\right)\right]. \tag{4}$$

With the tight bound of log-likelihood as objective function, we can further maximize the lower bound to find optimal posteriors of unobserved variables, i.e., LS, LF, and BD. As the output, the posterior probability of building damage, landslide, and liquefaction at each pixel will be jointly optimized with the causal coefficients of each edge in the Bayesian network. The computational cost depends on the number of pixels to be processed, which is ultimately determined by the satellite image resolutions and size of the covered seismic zone.

Evaluation is conducted for the Mw 6.4 earthquake in the southwest area of Puerto Rico on January 7, 2020 [9]. The reconnaissance team reported more than 775 affected buildings [12] and 800 ground failure observations induced by the earthquake [13]. DPMs are generated by the ARIA team using the SAR images from the Copernicus Sentinel-1 satellites of the European Space Agency [14]. Our estimation results are presented in Figure 2. Incorporating the DPM reduced the uncertainty in the posterior landslide model (*Fig. 2a)* with a 6% decrease in False Positive Rate, the posterior liquefaction model (*Fig. 2b, 2d)* with a 12.2% improvement in True Positive Rate, and the building damage posterior model (*Fig. 2c)* with a True Positive Rate of over 76%.

Conclusions

In this project, we introduce a novel causal graph-based Bayesian inference framework that integrates remote sensing data and geospatial models to enable accurate and high-resolution seismic ground failure and building damage estimates. Our framework can deal with large-scale and highly-complex multi-hazard scenarios and benefit rapid earthquake responses by providing accurate and high-resolution information about earthquake impacts. Through one holistic causal graph-based multi-layer Bayesian network, ground failure and building damage are modeled as categorical random variables and connected with causal dependencies. We jointly update the estimation of unobserved ground failure and building damage as well as their causal dependencies based on the prior ground failure models and DPMs. Our evaluation shows that integrating satellite images through Bayesian network improves ground failure estimation accuracy. The advantage of our approach is that the causal graph allows us to model more complex and nonlinear relationships among different variables and thus more accurately approximate their physical relationships. Furthermore, our approach is flexible to various scenarios without observed ground truth labels by using advanced machine learning techniques to approximate the posterior probability of ground failures and building damage from complex Bayesian networks.

References

[1] Xu C, Xu X, Yao X, Dai F (2014): Three (nearly) complete inventories of landslides triggered by the May 12, 2008 Wenchuan Mw 7.9 earthquake of China and their spatial distribution statistical analysis. Landslides, 11(3), 441-461.

[2] Quigley MC, Bastin S, Bradley BA (2013): Recurrent liquefaction in Christchurch, New Zealand, during the Canterbury earthquake sequence. Geology, 41(4), 419-422.

[3] Bird JF, Bommer JJ (2004): Earthquake losses due to ground failure. Engineering Geology, 75(2), 147-179.

[4] Nowicki Jessee MA, Wald DJ, Hamburger MW, Hearne M, Thompson EM (2014): Development of a globally applicable model for near real-time prediction of seismically induced landslides. Eng. Geol., 173, 54-65.

[5] Lee SARO (2005): Application of logistic regression model and its validation for landslide susceptibility mapping using GIS and remote sensing data. Int. J. Remote Sens., 26(7), 1477-1491.

[6] Karimzadeh, S., & Mastuoka, M. (2017). Building damage assessment using multisensor dual-polarized synthetic aperture radar data for the 2016 M 6.2 Amatrice Earthquake, Italy. Remote Sensing, 9(4), 330.

[7] Kundu S, Saha AK, Sharma DC, Pant CC (2013): Remote sensing and GIS based landslide susceptibility assessment using binary logistic regression model: A case study in the Ganeshganga Watershed, Himalayas. J. Indian Soc. Remote Sens., 41(3), 697-709.

[8] Geofabrik (2021): OpenStreetMap Data Extracts, available at http://download.geofabrik.de/osm/ (last accessed 29 August 2020).

[9] Xu S., Dimasaka J., Wald DJ, & Noh HY (2021, April). Fusing Damage Proxy Maps with Geospatial Models for Bayesian Updating of Seismic Ground Failure Estimations: A Case Study in Central Italy. In EGU General Assembly Conference Abstracts (pp. EGU21-13619).

[10] Allstadt KE, Thompson EM, Bayouth García D, Irizarry Brugman E, Hernandez JL, Schmitt RG, Hughes KS, Fuentes Z, Martinez SN, Cerovski-Darriau C, Perkins JP, Grant AR, Slaughter SL (2020): Field observations of ground failure triggered by the 2020 Puerto Rico earthquake sequence: U.S. Geological Survey data release, https://doi.org/10.5066/P96QNFMB.

[11] Knoper L, Allstadt KE, Clark MK, Thompson EM, Schmitt RG (2020): Inventory of landslides triggered by the 2020 Puerto Rico earthquake sequence: U.S. Geological Survey data release, https://doi.org/10.5066/P9U0IXLP.

[12] USGS (2020): M 6.4 - 8km S of Indios, Puerto Rico. U.S. Geological Survey, available at https://earthquake.usgs.gov/earthquakes/eventpage/us70006vll/executive (last accessed 28 January 2021).

[13] Federal Emergency Management Agency (FEMA) (2020): Puerto Rico M 6.4 Earthquake Preliminary Damage Assessments Dashboard, available at https://fema.maps.arcgis.com/apps/opsdashboard/index.html#/81e4b35ac91 041c4b7d408e740f9b324 (last accessed 14 October 2020).

[14] Advanced Rapid Imaging and Analysis (ARIA) – Center for Natural Hazards (2020): ARIA Data Share, available at https://aria-share.jpl.nasa.gov/20200106-Puerto_Rico_EQ/DPM/ (last accessed 26 October 2020).